Abdominal Imaging

Published online: 21 December 2014

Abdom Imaging (2015) 40:1843–1852
DOI: 10.1007/s00261-014-0333-4

Influence of the adaptive iterative dose reduction 3D algorithm on the detectability of low-contrast lesions and radiation dose repeatability in abdominal computed tomography: a phantom study

Jeong Hee Yoon,[1] Jeong Min Lee,[1,2] Bo Yun Hur,[3] Jeehyun Baek,[4] Hackjoon Shim,[5] Joon Koo Han,[1,2] Byung Ihn Choi[1,2]

[1]Department of Radiology, Seoul National University Hospital, Seoul, Korea
[2]Department of Radiology and Institute of Radiation Medicine, Seoul National University College of Medicine, 101 Daehak-ro, Jongno-gu, Seoul 110-744, Korea
[3]Department of Radiology, SMG-SNU Boramae Medical Center, Seoul, Korea
[4]Human Medical Imaging & Intervention Center, Seoul, Korea
[5]Toshiba Medical Systems Korea Co. Ltd, Seoul, Korea

Abstract

Purpose: The purpose of the study is to evaluate the influence of the adaptive iterative dose reduction (AIDR 3D) algorithm on the detectability of low-contrast focal liver lesions (FLLs) and the radiation dose repeatability of automatic tube current modulation (ATCM) in abdominal CT scans using anthropomorphic phantoms.
Materials and Methods: Three different sizes of anthropomorphic phantoms, each with 4 low-contrast FLLs, were scanned on a 320-channel CT scanner using the ATCM technique and AIDR 3D, at different radiation doses: full-dose, half-dose, and quarter-dose. Scans were repeated three times and reconstructed with filtered back projection (FBP) and AIDR 3D. Radiation dose repeatability was assessed using the intraclass correlation coefficient (ICC). Image noise, quality, and lesion conspicuity were assessed by four reviewers and the number of invisible FLLs was compared among different radiation doses and reconstruction methods.

Results: ICCs of radiation dose among the three CT scans were excellent in all phantoms (0.99). Image noise, quality, and lesion conspicuity in the half-dose group were comparable with full-dose FBP after applying AIDR 3D in all phantoms. In small phantoms, the half-dose group reconstructed with AIDR 3D showed similar sensitivity in visualizing low-contrast FLLs compared to full-dose FBP (P = 0.77–0.84). In medium and large phantoms, AIDR 3D reduced the number of missing low-contrast FLLs [3.1% (9/288), 11.5% (33/288), respectively], compared to FBP [10.4% (30/288), 21.9% (63/288), respectively] in the full-dose group.
Conclusion: By applying AIDR 3D, half-dose CT scans may be achievable in small-sized patients without hampering diagnostic performance, while it may improve diagnostic performance in medium- and large-sized patients without increasing the radiation dose.

Key words: Iterative reconstruction—AIDR 3D—Low-contrast detectability—Body size—Computed tomography

Electronic supplementary material: The online version of this article (doi:10.1007/s00261-014-0333-4) contains supplementary material, which is available to authorized users.

Correspondence to: Jeong Min Lee; *email:* jmsh@snu.ac.kr

Recently, the widespread utilization of computed tomography (CT) examinations has increased the con-

cerns over an already worrisome problem, medical radiation exposure [1–3]. To alleviate this potential risk in patients, several techniques have been developed to reduce this radiation exposure to patients, particularly in children, including the use of automatic tube current modulation (ATCM) [4] and iterative reconstruction (IR) [5, 6]. Among them, IR has drawn particular attention owing to its advantages over conventional filtered back projection (FBP) of decreased image noise and maintenance of image quality [7]. Until now, however, there have only been a few studies assessing the diagnostic performance of these techniques [8, 9]. Several studies have already shown that IR techniques can provide superior objective noise reduction compared with standard FBP, but controversy remains as to the range of exposure reduction able to be applied using these techniques while maintaining comparable diagnostic accuracy for the detection of focal lesions to standard dose FBP [8, 10–12].

In a continued effort to reduce radiation dose while maintaining image quality, adaptive iterative dose reduction (AIDR 3D), a commercial hybrid IR algorithm that reduces image noise and streak artifacts in the raw data and image space domain, has been developed [5, 13, 14]. However, although this hybrid IR algorithm has shown the capability of reducing noise while improving image quality [5, 13, 14], the diagnostic performance of low-contrast focal lesions was deemed not sufficient enough to support low-dose liver imaging; in fact, according to a recent phantom study, this hybrid IR algorithm was shown not to be able to preserve low-contrast detectability [9]. Indeed, the ability to detect low-contrast lesions is of unquestionable importance because lesions in abdominal solid organs including the liver usually show low-contrast while it shows high-contrast in the lung and CT colonography. However, in the previous study, they used only one phantom of one size, and only single IR strength was applied. In addition, owing to the phantom's shape, they applied a fixed tube current. This is different from what would be encountered in clinical practice as many hospitals often use a radiation dose modulation system. Considering that in addition to the IR algorithm used, the ATCM technique and patients' body habitus are also significant factors affecting the detectability of focal lesions in abdominal solid organs, we believe that the influence of IR techniques on the detectability of low-contrast lesions in different body sizes, as well as the radiation dose repeatability of ATCM should be explored.

Therefore, the purpose of this study is to evaluate the influence of the AIDR 3D algorithm on the detectability of low-contrast lesions and the radiation dose repeatability of ATCM in combination with AIDR 3D in abdominal CT scans using anthropomorphic phantoms simulated for different body sizes.

Materials and methods

Phantom preparation

A customized anthropomorphic phantom (PH-5, Kyoto Kagaku), which was used for our previous study [15], was prepared to imitate the upper abdomen during the portal venous phase (Fig. 1A). The longest and shortest diameters of the phantom were 26 and 18 cm, and the abdominal circumference was 79 cm. To mimic the different sizes of the human torso, three different sizes of phantoms were created by wrapping the anthropomorphic phantom with pork fat: 2.5 cm in thickness to mimic a medium-sized human torso (medium-sized phantom) and 5 cm in thickness to mimic a large-sized human torso (large-sized phantom) (Fig. 1B, C). The abdominal circumferences were approximately 85, and 101 cm in the medium and large phantoms, respectively. In each phantom, a total of eight focal liver lesions (FLLs), 1.5 cm in diameter, were placed (Fig. 2). The FLLs were comprised of four high-contrast lesions (lesion-to-liver contrast: ±30, ±50) and four low-contrast lesions (lesion-to-liver contrast: ±10, ±20).

CT acquisition and image reconstruction

CT acquisition. The three anthropomorphic phantoms were scanned using a 320-channel multidetector CT scanner craniocaudally, in the supine position (Aquilion ONE; Toshiba Medical Systems, Tokyo, Japan). All scans were performed under the following condition based on our routine abdominal CT protocol: 120 kVp; collimation 0.5 mm; slice thickness 3.0 mm; with ATCM. The Toshiba CT scanner uses a combined system of AIDR 3D and the ATCM technique (Sure Exposure 3D, Toshiba Medical Systems), and therefore, dose modulation was determined by two factors, noise level (specified in terms of the selected standard deviation (SD) of CT numbers measured in a patient-equivalent water phantom) and the reconstruction algorithm used (FBP vs. AIDR 3D). When FBP is used with Sure Exposure 3D, tube current was determined by predetermined the image quality, which is specified in terms of selected SD of CT numbers measured in a patient-equivalent water phantom [16]. However, when AIDR 3D and Sure Exposure 3D are used together, radiation dose is automatically reduced after using AIDR 3D compared to FBP, as AIDR 3D is able to reduce image noise [17]. In our study, in order to determine the influence of AIDR 3D on the radiation dose repeatability of ATCM in different body habitus, three different reconstruction techniques [filtered back projection (FBP) scanning, mild (MILD) scanning, standard (STD) scanning] were used at four different noise levels (SD: 13, 15, 17, and 19), forming twelve different combinations of CT scan parameters. CT scans with the same scanning

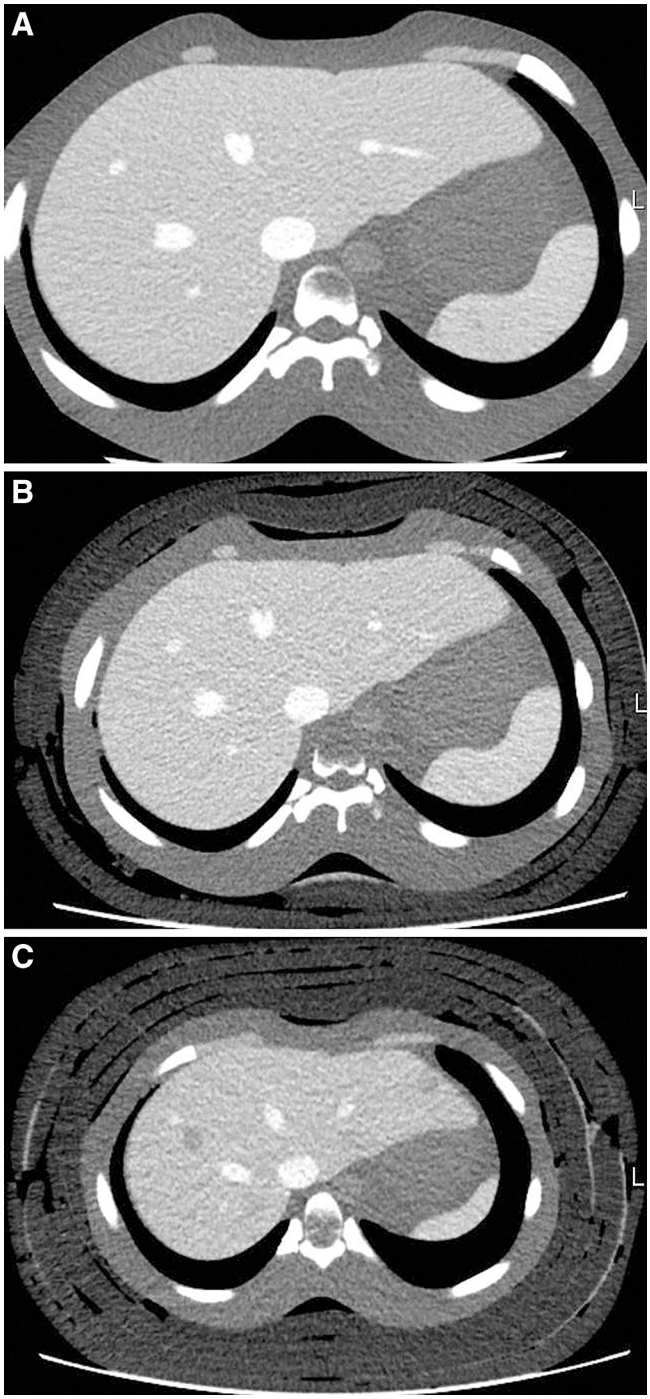

Fig. 1. Computed tomography (CT) scans of anthropomorphic phantoms of different sizes. Images of small (**A**), medium (**B**) and large-sized (**C**) phantoms are shown, taken using 120 kVp at full-dose (FD, filtered back projection scan mode and noise level 13), and reconstructed using mild strength of AIDR 3D.

parameters were performed three times in each phantom, successively after placing the phantom completely down on the table to obtain the scan from the very beginning. Therefore, a total of 36 scans were acquired for each phantom: twelve different conditions with three repeated scans for each condition.

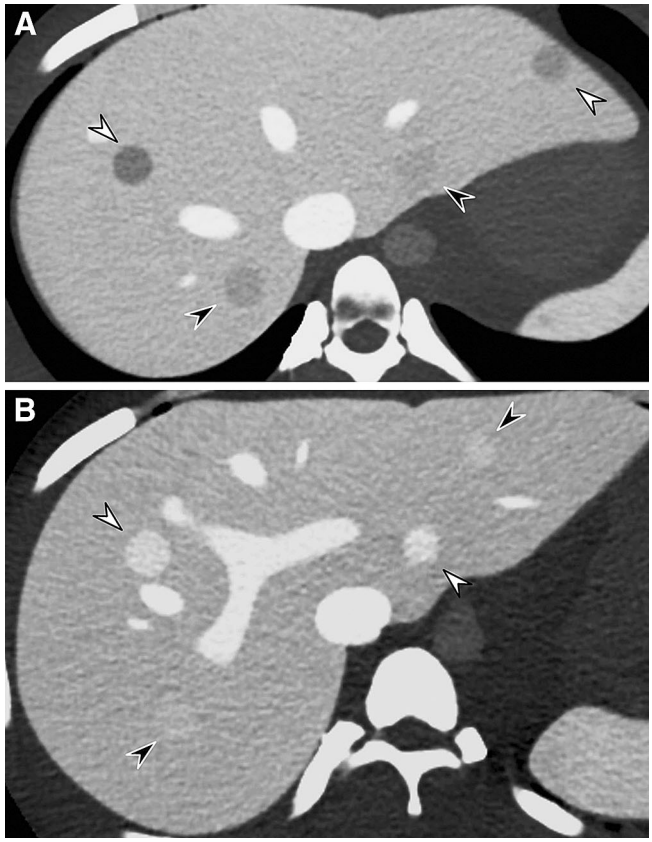

Fig. 2. CT images of eight focal liver lesions (FLLs) in the anthropomorphic phantom. Four hypoattenuating (**A**) and four hyperattenuating FLLs (**B**) were placed in the phantom. Four low-contrast FLLs (*black arrowheads*) and four high-contrast FLLs (*white arrowheads*) are marked.

Image reconstruction. Each CT scan was reconstructed using four different reconstruction algorithms: FBP and three strengths of hybrid IR algorithms [MILD, STD and strong (STR)]. The same soft tissue kernel (FC 08) was used for all scans.

Radiation dose calculation and dividing groups based on radiation dose

The volume CT dose index ($CTDI_{vol}$) and the dose-length product (DLP) were recorded for each radiation dose group in the three phantoms. After calculating the radiation doses of each CT scan, CT scans were divided into three groups: full-dose (FD), half-dose (HD), and quarter-dose (QD) groups for each phantom. The target radiation doses of each group were 100% in FD, 50% of FD in HD, and 25% of FD in the QD group. Scans with highly deviated radiation doses ($>15\%$) from the target dose were excluded so as to lower the standard deviation of radiation doses in each group. In scans with a borderline difference (11–15%), they were either included or excluded from the group, toward minimizing the difference between the average radiation dose and the target

dose of the group. Finally, four scans each in small and large phantoms and two scans in a medium phantom were excluded (Supplement 1). Target doses and achieved doses in each dose group of each phantom are summarized in Supplement 1. Target doses and achieved doses were similar in all radiation dose groups, but the HD group in the small-sized phantom showed 10% higher radiation dose than the target dose (60.5% vs. 50%) as radiation doses of most scans in the small-sized phantom were deviated from 50% of the radiation dose in the FD group (Supplement 1).

Image analysis

A total of 432 image sets (3 phantoms* 3 scanning levels* 4 noise levels* 4 reconstruction types*3 repeated scans) were obtained. These image sets were divided into three groups in a random manner and reviewed at 2 week intervals to avoid reviewers' fatigue and learning bias. In addition, the orders of image sets in each group were also randomly distributed. All image reviews were performed with picture archiving and communication system (PACS) (Maroview 5.4, Infinitt, Seoul, Korea) using monitors with a spatial resolution of 1,600 × 1,200. During the review, the observers were allowed to change window width and level as they would in clinical practice.

Lesion conspicuity. Four abdominal radiologists (B.Y.H., J.H.Y., J.B., and J.M.L. with six, eight, eleven and twenty one years of experience in abdominal CT interpretation, respectively) evaluated the CT data independently. Although all reviewers were blinded to the scan parameters and reconstruction methods, all phantoms had FLLs in the same location and the reviewers were expected to become aware of the presence of FLLs. Therefore, we gave each FLL an identification number from one to eight (FLL1 to 8). The readers were then asked to grade the level of conspicuity of each FLL as follows: grade 1, definitely not seen; grade 2, may present; grade 3, probably present; and grade 4, definitely present.

Qualitative image quality evaluation. Independent qualitative image analysis was performed by two abdominal radiologists (B.Y.H., and J.B.). After independent review, a joint review was performed until both reviewers reached a consensus on all borderline cases. Image noise and overall image quality were assessed on a four-point scale. For image noise, a score of 1 indicated unacceptable noise; score 2, significant image noise, affecting diagnostic performance; score 3, presence of image noise with decreased image quality, but diagnostically acceptable; and score 4, minimal or no significant image noise, without decreasing image quality [18]. For image quality evaluation, a score of 1 suggested a diagnostically unacceptable image; score 2, poor than average; score 3, average; and score 4, better than average image quality [19, 20].

Quantitative image noise and lesion conspicuity evaluation. One attending radiologist (J.H.Y.) measured the CT numbers and image noise by drawing regions of interest (ROIs; mean size, 106.2 ± 23.9 mm^2). All image sets of each phantom were displayed side-by-side, and the ROIs were copied and pasted on each image. Image noise was measured in the subcutaneous fat layer and both paraspinal muscles, and the average value was used to indicate image noise. In addition, the CT number of the liver was measured three times in the left lateral, right anterior, and right posterior segments of the liver and the average value of the three measurements was utilized as the liver attenuation of the image set. CT numbers of the FLLs were measured by drawing ROIs at the slice showing the largest dimension of FLLs. Contrast-to-noise ratio (CNR) of each FLL was calculated as follows: $CNR = (ROI_{liver} - ROI_{FLL})/\text{image noise}$ [17].

Statistical analysis

The radiation dose repeatability of the combination of the ATCM technique and AIDR 3D was assessed using intraclass correlation coefficients (ICC) among the three scans. With regard to image quality, image noise, CNRs, and image quality of the different reconstruction algorithms at the same radiation doses were compared using an analysis of variance for repeated measurements (RMANOVA) or Friedman analysis of variance. The effect of different radiation doses on image noise and quality, as well as the effect of different reconstruction algorithms were also assessed in the same manner. Post hoc tests were performed when there was a significant difference between groups after RMANOVA or Friedman analyses. As for lesion conspicuity, one-way Analysis of variance (ANOVA) as performed to compare image sets of four reconstruction types in HD and QD groups with the FBP images of FD group while a combination of radiation doses and reconstruction methods were treated as a variance factor. To determine the incidence of 'invisible' FLLs among the reconstruction methods, the χ^2 test was performed.

Agreement between the readers was graded as follows: A κ value of less than 0.20 indicated poor agreement; a κ value of 0.21–0.40, fair agreement; a κ value of 0.41–0.60, moderate agreement; a κ value of 0.61–0.80, good agreement; and a κ value of 0.81–1.00, very good agreement. All statistical tests were performed using commercially available software (IBM SPSS, version 19, SPSS Inc., IBM Company, Armonk, NY, USA; Medcalc, Medcalc Software, Mariakerke, Belgium). A P-value <0.05 was considered to indicate a significant difference.

Results

Influence of AIDR 3D on radiation dose repeatability and dose reduction

DLPs and CTDIvol of each scan depending on the scan setting and noise level are summarized in Supplement 2. The radiation doses were not the same according to the three repeated scan data, but showed excellent agreements in all phantoms (Fig. 3): ICC values were 0.99 in the small-sized phantom (95% CI 0.967–0.996), 0.997 in the medium-sized phantom (95% CI 0.991–0.999), and 0.995 in the large-sized phantom (ICC: 0.995; 95% CI 0.986–0.998). In all phantoms, radiation doses significantly decreased by combining increasing noise levels (SD) and changing the scan type from FBP to MILD or STD; up to 86.6, 83.9, and 78.6% of DLP reduction were achieved in small, medium, and large phantoms (Fig. 4, Supplement 2). Adjusting the scan type decreased radiation doses further than changing the SD level; in a small phantom, switching scan type from FBP to STD reduced 71.7% of DLP at SD of 13, but increasing SD from 13 to 19 reduced 37.8% of DLP (Fig. 4, Supplement 2).

Comparison of image noise and image quality of AIDR 3D images to FBP images

On qualitative analysis, noises of HD MILD, STD and STR images did not show significant differences compared to FD FBP images in all three phantoms (P = 0.087–1.0, Table 1). However, QD images showed significantly noisier images compared to FD FBP images in all phantoms (P < 0.0001–0.045) except STR reconstruction images (P = 0.055–1.0, Table 1). As for image quality, HD AIDR reconstructed images showed comparable image quality with FD FBP images in all phantoms (P = 0.055–1.0, Table 1) except HD MILD reconstruction images in the medium-sized phantom (3.67 ± 0.52 in FD FBP vs. 2.93 ± 0.46 in HD MILD, P = 0.046). However, QD images tended to show lower image quality regardless of image reconstruction, compared to FD FBP images in all phantoms (P < 0.0001–0.048, Table 2). Two reviewers showed moderate inter-observer agreement in noise evaluation (κ = 0.52) and good agreement in image quality assessment (κ = 0.69).

On quantitative evaluation, AIDR 3D decreased image noise compared to FBP in all phantoms (Supplements 3–4). Noise reduction was more substantial as phantom size increased and as radiation dose decreased (Supplement 4).

Conspicuity of Low-contrast FLLs depending on radiation dose, reconstruction algorithms, and phantom size

The lesion conspicuity of FLLs is summarized in Table 3 and CNRs of each FLL are presented in Supplement 5.

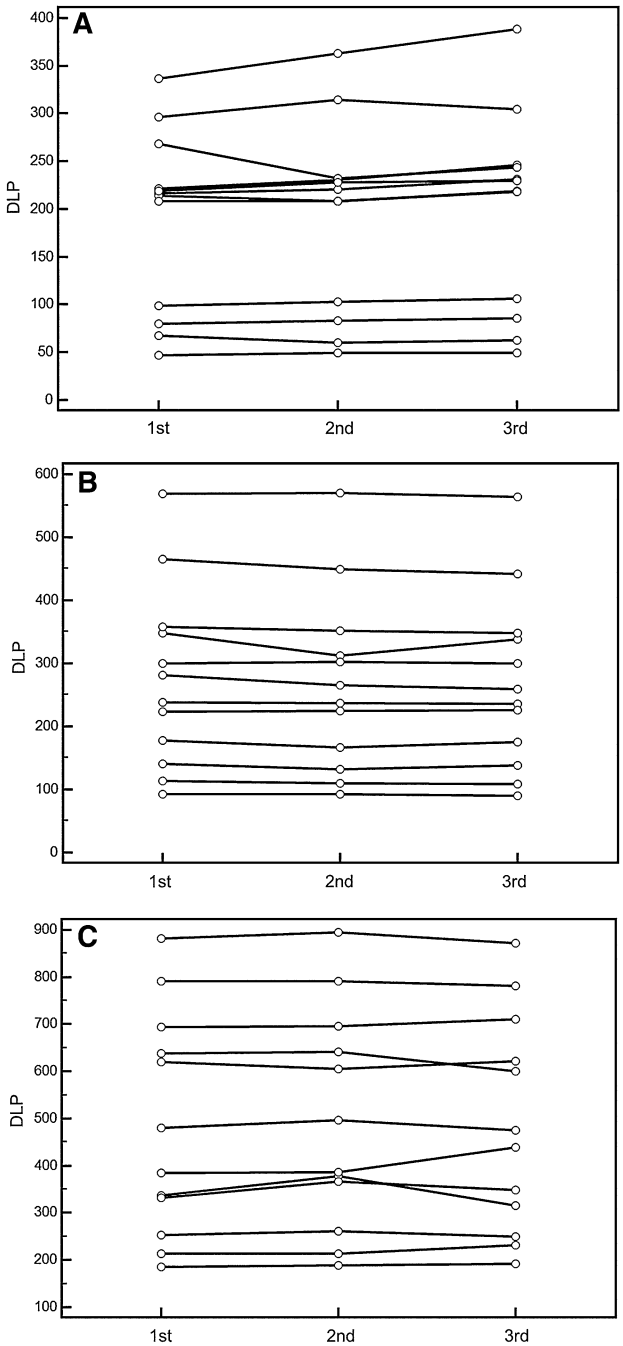

Fig. 3. Graphs showing dose-length products (DLP) of each phantom in three repeated scans. Each phantom was scanned with 12 different radiation dose modulation settings, and each setting was repeated three times. *Dots* connected with *lines* indicate the same dose modulation setting. DLPs were similar through all three different scans in small- (**A**), medium- (**B**) and large-sized (**C**) phantoms.

In comparison to the FBP images of each radiation dose group, lesion conspicuity of low-contrast FLLs significantly decreased as radiation dose decreased in medium and large phantoms (Table 3). However, after AIDR 3D reconstruction, HD images did not show a significant

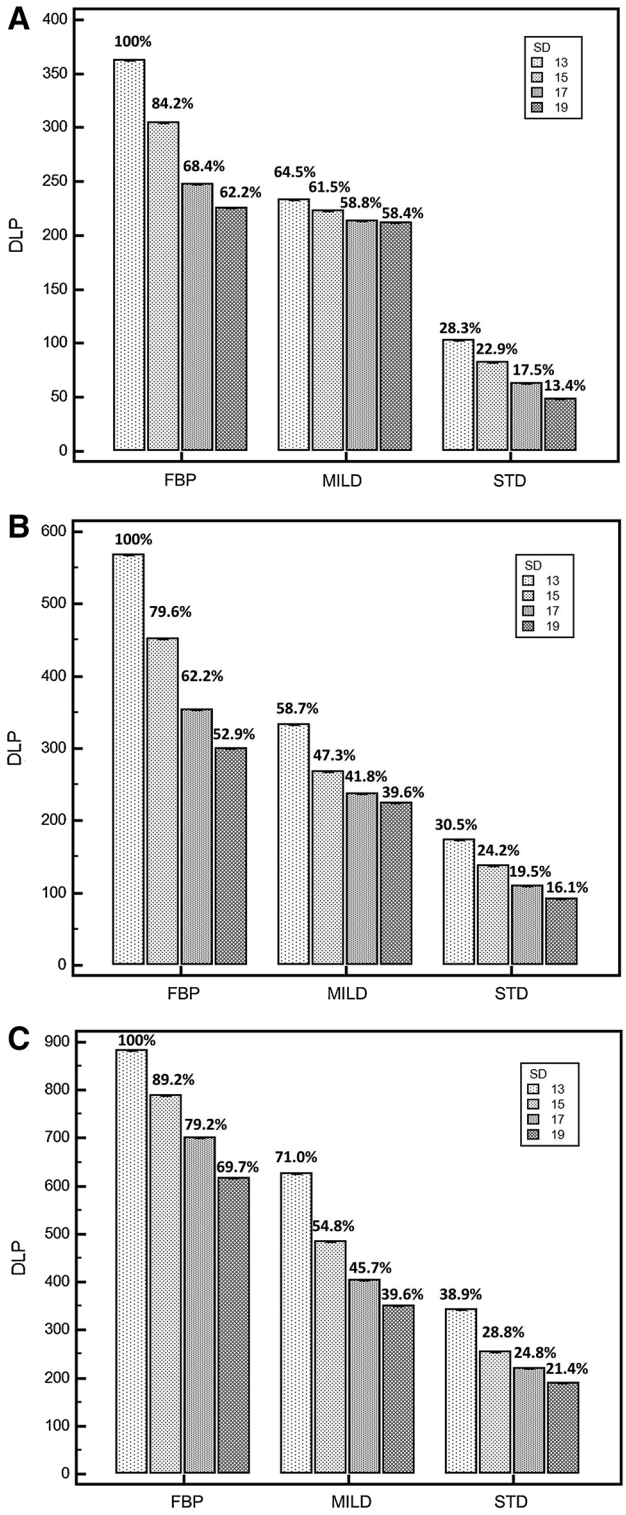

◀**Fig. 4.** Graphs showing DLPs using different scanning parameters for each phantom. X-axis indicates the scanning mode and y-axis indicates DLP. *Different colors* of *bars* indicate different noise levels. By adjusting scan modes, DLP significantly decreased in small- (**A**), medium- (**B**) and large-sized (**C**) phantoms. Radiation dose reduction was more substantial when adjusting the scan mode than the image noise level. Percentages of each column indicate DLP proportion, compared to FBP with noise level of 13. *FBP* filtered back projection, *MILD* mild strength of scanning mode, *STD* standard strength of scanning mode.

Table 1. Qualitative image noise assessment according to phantom size and reconstruction method

	Reconstruction type			
	FBP	MILD	STD	STR
Small				
FD	4.00 ± 0.00	4.00 ± 0.00	4.00 ± 0.00	4.00 ± 0.00
P-value†	–	*1.0*	*1.0*	*1.0*
HD	3.07 ± 0.26	3.53 ± 0.52	3.67 ± 0.49	3.80 ± 0.41
P-value†	*0.033*	*0.142*	*0.467*	*0.529*
QD	2.17 ± 0.41	2.67 ± 0.52	2.67 ± 0.52	2.83 ± 0.75
P-value†	*0.001*	*0.020*	*0.020*	*0.055*
Medium				
FD	4.00 ± 0.00	4.00 ± 0.00	4.00 ± 0.00	4.00 ± 0.00
P-value†	–	*1.0*	*1.0*	*1.0*
HD	3.00 ± 0.00	3.47 ± 0.46	3.53 ± 0.52	3.73 ± 0.46
P-value†	*<0.0001*	*0.124*	*0.534*	*1.0*
QD	2.11 ± 0.33	2.78 ± 0.44	2.89 ± 0.33	3.00 ± 0.00
P-value†	*<0.0001*	*0.006*	*0.020*	*0.063*
Large				
FD	3.50 ± 0.55	3.67 ± 0.52	3.83 ± 0.41	3.83 ± 0.41
P-value†	–	*1.00*	*0.999*	*0.999*
HD	2.78 ± 0.44	3.22 ± 0.44	3.44 ± 0.53	3.56 ± 0.53
P-value†	*0.087*	*1.00*	*1.0*	*1.00*
QD	1.33 ± 0.50	2.33 ± 0.53	2.67 ± 0.50	2.89 ± 0.06
P-value†	*<0.0001*	*0.006*	*0.045*	*0.369*

Values are mean ± standard deviation. †Difference in score of the 11 image sets compared to FD FBP images. A *P*-value less than 0.05 indicates statistical significance

difference compared to FD FBP images in all three phantoms ($P = 0.092$–1.0, Table 3). In addition, the lesion conspicuity of low-contrast FLLs was significantly worse in the QD group compared to the FD FBP group, regardless of the reconstruction algorithms used in all phantoms ($P < 0.0001$, Table 3). In FD FBP group, lesion conspicuity significantly decreased as phantom size increased among the three phantoms: 2.8 ± 0.9 in the small-sized phantom, 2.6 ± 0.9 in the medium-sized phantom, and 2.1 ± 0.9 in the large-sized phantom ($P < 0.0001$). Only the large-sized phantom showed a statistically significant improvement of low-contrast FLL conspicuity after AIDR 3D reconstruction at FD ($P = 0.034$ in STD reconstruction, 0.031 in STR reconstruction), whereas the small- and medium-sized phantoms showed similar lesion conspicuity on AIDR 3D reconstruction images with those on FBP images at FD.

In addition, the numbers of invisible low-contrast FLLs were compared among different reconstruction strengths (Table 4). The number of invisible low-contrast FLLs significantly increased as radiation dose decreased ($P = 0.005$, Table 4). Especially in the QD groups of the three phantoms, the number of invisible low-contrast FLLs was significantly higher in the QD groups in all

three phantoms compared to the number of invisible FLLs in the FD FBP images ($P < 0.0001$, Table 4). In the comparison between HD AIDR 3D images and FD FBP images, the number of invisible low-contrast FLLs varied depending on the phantom size. In the small-sized phantom, there were no significant differences in the number of invisible FLLs between FD FBP images and HD AIDR 3D images (Fig. 5, MILD, STD and STR, $P = 0.77$–0.84). However, in the medium-sized phantom, HD AIDR 3D images showed a significantly higher number of invisible low-contrast FLLs compared to FD FBP images ($P < 0.0001$, Table 4). In the large-sized phantom, the number of missing lesions exceeded 20% in FD FBP images [21.9% (63/288), Table 4], and the high missing rate was improved after applying AIDR 3D [12.5% (36/288) with STD reconstruction, 11.5 (33/288) with STR reconstruction, Table 4]. All high-contrast FLLs showed better lesion conspicuity than low-contrast FLLs in the same scan and reconstruction condition. All high-contrast FLLs showed higher scores of lesion conspicuity than 3.0 on average, and was sufficient enough to be detected regardless of phantom size, radiation dose and reconstruction algorithm (Table 3).

Table 2. Image quality assessment according to phantom size, radiation dose, and reconstruction method

	Reconstruction type			
	FBP	MILD	STD	STR
Small				
FD	4.00 ± 0.00	4.00 ± 0.00	4.00 ± 0.00	4.00 ± 0.00
P-value†	*	*	*	*
HD	3.00 ± 0.00	3.13 ± 0.35	3.53 ± 0.52	3.80 ± 0.41
P-value†	*0.013*	*0.055*	*0.135*	*0.521*
QD	1.83 ± 0.41	2.00 ± 0.00	2.33 ± 0.52	2.50 ± 0.55
P-value†	*0.003*	*0.009*	*0.013*	*0.037*
Medium				
FD	3.67 ± 0.52	3.83 ± 0.41	4.00 ± 0.00	4.00 ± 0.00
P-value†	–	*1.0*	*0.966*	*0.966*
HD	2.67 ± 0.49	2.93 ± 0.46	3.27 ± 0.59	3.47 ± 0.52
P-value†	*0.002*	*0.046*	*1.0*	*1.0*
QD	1.78 ± 0.44	2.22 ± 0.44	2.67 ± 0.50	2.89 ± 0.33
P-value†	*<0.0001*	*<0.0001*	*0.001*	*0.021*
Large				
FD	3.17 ± 0.41	3.67 ± 0.52	3.83 ± 0.41	3.83 ± 0.41
P-value†	–	*0.915*	*0.421*	*0.421*
HD	2.22 ± 0.44	2.78 ± 0.44	3.00 ± 0.00	3.44 ± 0.53
P-value†	*0.014*	*0.955*	*1.0*	*1.0*
QD	1.22 ± 0.44	2.22 ± 0.44	2.22 ± 0.44	2.44 ± 0.53
P-value†	*<0.0001*	*0.004*	*0.004*	*0.048*

Values are mean ± standard deviation. †Difference in score of the 11 image sets compared to scores on FD FBP images. A *P*-value less than 0.05 indicates statistical significance. * No available results, due to standard deviation value of zero (SD = 0)

Discussion

Our study results demonstrated that image noise, image quality, and lesion conspicuity of low-contrast FLLs were improved after applying AIDR 3D in all three different sized phantoms at the same radiation dose. This image quality improvement provided by AIDR 3D allowed a radiation dose reduction of up to 50%, providing comparable image quality to full-dose FBP images. Furthermore, as for the conspicuity of low-contrast FLLs, AIDR 3D images in the HD group showed similar scores with the FD FBP groups in all phantoms, while AIDR 3D at QD showed worse lesion conspicuity than

Table 3. Lesion conspicuity of each phantom according to lesion contrast, radiation dose, and reconstruction method

	Low-contrast				High-contrast			
	FBP	MILD	STD	STR	FBP	MILD	STD	STR
Small								
FD	2.8 ± 0.9	2.9 ± 0.9	3.0 ± 0.8	2.9 ± 0.9	3.9 ± 0.4	3.9 ± 0.4	3.9 ± 0.4	3.9 ± 0.4
P-value†	–	*1.0*	*1.0*	*1.0*	–	*1.0*	*1.0*	*1.0*
HD	2.6 ± 0.9	2.8 ± 0.9	2.8 ± 0.9	2.8 ± 0.9	3.9 ± 0.4	3.8 ± 0.4	3.9 ± 0.4	3.9 ± 0.4
P-value†	*1.0*	*1.0*	*1.0*	*1.0*	*1.0*	*1.0*	*1.0*	*1.0*
QD	1.8 ± 0.7	2.1 ± 0.8	2.2 ± 0.8	2.2 ± 0.9	3.6 ± 0.5	3.7 ± 0.5	3.7 ± 0.5	3.7 ± 0.5
P-value†	*<0.0001*	*0.002*	*0.003*	*0.023*	*0.008*	*0.598*	*0.428*	*0.428*
Medium								
FD	2.6 ± 0.9	2.7 ± 0.9	2.8 ± 0.9	2.8 ± 0.9	3.9 ± 0.4	3.9 ± 0.4	3.9 ± 0.4	3.9 ± 0.3
P-value†	–	*1.0*	*1.0*	*1.0*	–	*1.0*	*1.0*	*1.0*
HD	2.1 ± 0.9	2.3 ± 0.9	2.4 ± 0.9	2.4 ± 0.9	3.8 ± 0.5	3.8 ± 0.5	3.8 ± 0.5	3.8 ± 0.5
P-value†	*0.001*	*0.539*	*0.987*	*0.999*	*0.356*	*0.909*	*0.580*	*0.750*
QD	1.6 ± 0.6	1.9 ± 0.8	2.0 ± 0.8	2.0 ± 0.8	3.5 ± 0.5	3.6 ± 0.5	3.7 ± 0.5	3.7 ± 0.5
P-value†	*<0.0001*	*<0.0001*	*<0.0001*	*<0.0001*	*<0.0001*	*0.001*	*0.005*	*0.034*
Large								
FD	2.1 ± 0.9	2.4 ± 0.9	2.5 ± 0.9	2.5 ± 0.9	3.7 ± 0.5	3.7 ± 0.5	3.8 ± 0.4	3.8 ± 0.4
P-value†	–	*0.935*	*0.034*	*0.031*	–	*1.0*	*1.0*	*1.0*
HD	1.8 ± 0.8	2.0 ± 0.9	2.1 ± 0.9	2.1 ± 0.9	3.5 ± 0.5	3.6 ± 0.5	3.6 ± 0.5	3.6 ± 0.5
P-value†	*0.092*	*1.0*	*1.0*	*1.0*	*1.0*	*1.0*	*1.0*	*1.0*
QD	1.4 ± 0.6	1.6 ± 0.7	1.7 ± 0.7	1.7 ± 0.7	3.2 ± 0.7	3.4 ± 0.5	3.5 ± 0.5	3.5 ± 0.5
P-value†	*<0.0001*	*<0.0001*	*0.001*	*0.002*	*<0.0001*	*0.007*	*0.547*	*0.844*

Values are mean ± standard deviation. †Difference in score of the 11 image sets compared to FD FBP images. A *P*-value less than 0.05 indicates statistical significance

Table 4. Number of low-contrast FLLs which were not visualized on the review sessions according to radiation doses and reconstruction algorithms

	FBP	MILD	STD	STR
Small				
FD (n = 144)	6 (4.2%)	0 (0%)	0 (0%)	0 (0%)
P-value†	–	*0.038*	*0.038*	*0.038*
HD (n = 720)	93 (12.9%)	36 (5.0%)	30 (4.2%)	24 (3.3%)
P-value†	*0.005*	*0.84*	*0.82*	*0.77*
QD (n = 288)	108 (37.5%)	90 (31.3%)	84 (29.2%)	84 (29.2%)
P-value†	*<0.0001*	*<0.0001*	*<0.0001*	*<0.0001*
Total (n = 1152)	207(18.0%)	126 (10.9%)	114 (9.9%)	108 (9.4%)
Medium				
FD (n = 288)	30 (10.4%)	18 (6.3%)	15 (5.2%)	9 (3.1%)
P-value†	–	*0.104*	*0.03*	*<0.0001*
HD (n = 720)	225 (31.3%)	174 (24.2%)	153 (21.3%)	153 (21.3%)
P-value†	*<0.0001*	*<0.0001*	*<0.0001*	*<0.0001*
QD (n = 396)	201 (50.8%)	144 (36.4%)	144 (36.4%)	138 (34.8%)
P-value†	*<0.0001*	*<0.0001*	*<0.0001*	*<0.0001*
Total (n = 1404)	456 (32.5%)	336 (23.9%)	312 (22.2%)	300 (21.3%)
Large				
FD (n = 288)	63 (21.9%)	54 (18.8%)	36 (12.5%)	33 (11.5%)
P-value†	–	*0.41*	*0.004*	*0.0012*
HD (n = 432)	144 (33.3%)	129 (29.9%)	114 (26.4%)	105 (24.3%)
P-value†	*0.0012*	*0.02*	*0.199*	*0.511*
QD (n = 432)	279 (64.6%)	216 (50%)	180 (41.7%)	174 (40.3%)
P-value†	*<0.0001*	*<0.0001*	*<0.0001*	*<0.0001*
Total (n = 1152)	486 (42.2%)	399 (34.6%)	330 (28.6%)	312 (27.1%)

Percentage in parentheses are proportion of undetected low-contrast FLLs to total number of low-contrast FLLs. †Difference in number of invisible FLLs compared to FD FBP images. A *P*-value less than 0.05 indicates statistical significance

that of FD FBP. Therefore, based on our observations, a radiation dose reduction of up to 50% could be obtained while maintaining acceptable image quality with the use of the AIDR 3D algorithm, while very low-dose imaging using the hybrid IR technique may not be a realistic option at abdominal CT for the evaluation of solid organs. However, although HD images reconstructed with AIDR 3D in the small-sized phantom showed a similar number of missing low-contrast FLLs with FD FBP images, the number of missing low-contrast FLLs was similar or even increased in the HD group regardless of the reconstruction method in the medium- and large-sized phantoms. Thus, based on these results, we believe that AIDR 3D CT images at 50% dose reduction may possess a risk of reducing the diagnostic performance of CT in detecting low-contrast FLLs in patients with medium and large body habitus.

In recent years, with the development of clinically available IR techniques from major CT vendors allowing the reduction of image noise, radiation dose reduction has been actively investigated using various IR techniques. Indeed, in the setting of high lesion-to-background contrast such as in chest CT and CT colonography, the diagnostic performance of these techniques in detecting focal lesions was not hampered [21, 22]. Several studies using abdominal CT also reported that the detectability of FLLs such as hepatocellular carcinoma was less hampered by low radiation dose [7, 18, 20]. In fact, until now, whether or not IR images at HD could provide equivalent diagnostic performance for detecting low-contrast liver lesions such as liver metastases compared to FBP images at regular dose remains controversial. In our study, the possible upper limit of radiation dose reduction might be 50% of FD in our small-sized phantom, while it should be less than 50% in a medium- or large-sized phantom. Our study results are in good agreement with the results of previous studies on IR techniques [10, 14]. Applying the results of one previous study on the correlation between body mass and body circumference [21], the small phantom used in our study with a 79 cm circumference, would be equivalent to a patient weighing approximately 60–65 kg, and the medium- and large-sized phantoms would be equivalent to a 70–75 kg patient and 85–90 kg patient, respectively. Based on this correlation, we should be able to reduce the radiation dose in patients under 65 kg, whereas in patients over 70 kg, we should maintain the standard radiation dose and avoid aggressive radiation dose reduction to preserve the detectability of liver CT scans for low-contrast FLLs. Instead, we believe that in patients with medium and large body habitus, the application of AIDR 3D may have the potential to improve diagnostic performance in detecting low-contrast FLLs at a standard radiation dose compared with FBP images.

Contrary to the positive findings above, our results also showed that the hybrid IR algorithm seemed to have a limited capacity in maintaining or improving diagnostic performance for the detection of low-contrast FLLs at lower radiation dose settings (>50%). The discrepancy between marked noise improvement and hampered low-contrast FLL detectability might be explained by the non-linearity of today's IR algorithms,

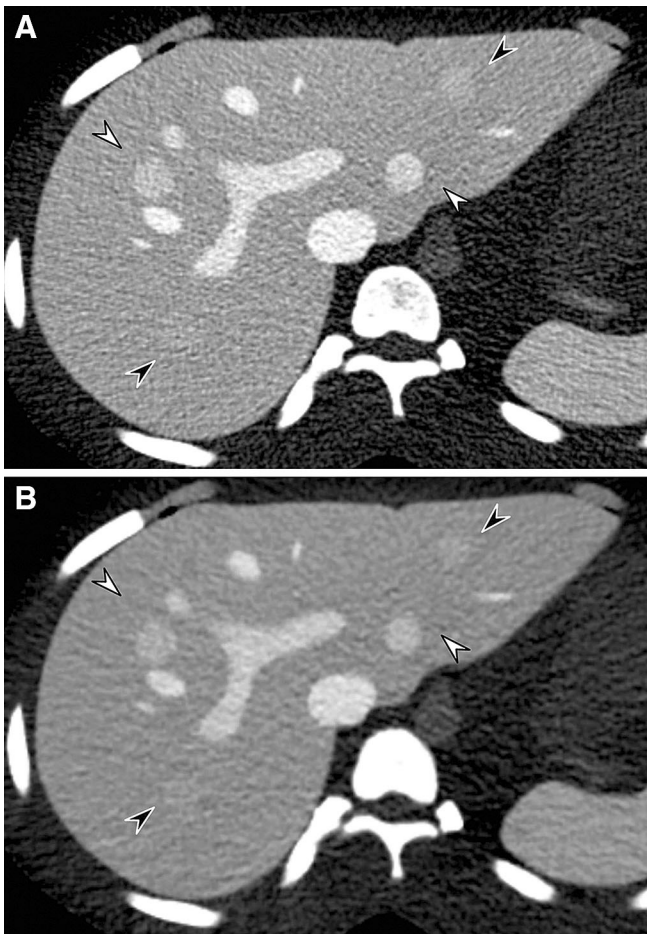

Fig. 5. CT images of a small anthromorphic phantom. Both of FD FBP images (**A**) and HD STR images (**B**) demonstrated two low-contrast (*black arrowheads*) and high-contrast (*white arrowheads*) FLLs similarly.

whereas FBP shows linearity and clear trades-off between image noise, texture, and image quality. An altered noise power spectrum and image texture may also have played a role in hampering the diagnostic performance of IR techniques for the detection of low-contrast FLLs at lower radiation dose. In addition, the lower diagnostic performance might also be attributed to insufficient noise suppression with hybrid IR, considering that there was one report of improved low-contrast lesion detection using a pure IR technique.

Finally, we also evaluated the radiation dose repeatability of Sure Exposure 3D, which is able to adjust the tube current to achieve a target image quality under different acquisition and reconstruction parameters. It also has a unique feature in that it is fully integrated into AIDR 3D [14], and as AIDR 3D is used together with Sure Exposure program, it should simplify the workflow and would be theoretically less affected by image smoothing with radiation dose reduction [22]. However, as users must define the scanning parameters, noise level and the reconstruction method to be used in order to achieve satisfying image quality with low radiation dose, it is a bit challenging to predict the changes of radiation dose in clinical practice. Thus, there was a need to test the radiation dose repeatability of this technique and to observe how radiation dose changes after adjusting the scan parameters for various sizes of phantoms. According to our observation, the system showed excellent repeatability of radiation dose determination. In addition, adjusting scanning modes showed considerable more effect than adjusting noise levels at the same scan mode in reducing radiation dose. Our results on lesion detection, image quality, and dose reduction after adjusting the parameters for differently sized phantoms would provide valuable information and may help operators optimize the scan setting for each individual patient.

Our study has several limitations. First, instead of assessing lesion detectability directly, we assessed lesion conspicuity and the number of 'invisible' FLLs in each image because of the fixed location of FLLs. Therefore, we should be cautious when applying these results to human patients directly. Second, we did not evaluate the lesion detectability according to lesion size as all FLLs in our study were of the same size (1.5 cm). Third, because we used the same phantoms in repetitive reviews, there may have been recall bias. However, in an effort to minimize the bias, we randomly distributed the image sets and scheduled a two-week interval between readings. Fourth, we did not investigate the possibility of mild dose reduction (20–30%) in medium and large phantoms, without hampering diagnostic performance. Despite of these limitations, we believe that this study has value as we investigated the influence of radiation dose, reconstruction method, and body habitus on the detection of low-contrast FLLs under automatic dose modulation, as in clinical practice, after confirming radiation dose repeatability.

In conclusion, ATCM including AIDR 3D showed significantly high inter-scan repeatability. In addition, the application of hybrid IR may reduce the radiation dose up to 50% in patients with small body habitus without hampering low-contrast detectability. In medium- and large-sized patients, hybrid IR may serve as a tool to improve diagnostic performance in detecting low-contrast FLLs using the standard radiation dose.

Conflict of interest H.S. is an employee of Toshiba Medical Systems Korea.

References

1. Sodickson A, Baeyens PF, Andriole KP, et al. (2009) Recurrent CT, cumulative radiation exposure, and associated radiation-induced cancer risks from CT of adults. Radiology 251:175–184
2. Smith-Bindman R, Lipson J, Marcus R, et al. (2009) Radiation dose associated with common computed tomography examinations and the associated lifetime attributable risk of cancer. Arch Intern Med 169:2078–2086

3. Berrington de Gonzalez A, Mahesh M, Kim K-P, et al. (2009) Projected cancer risks from computed tomographic scans performed in the United States in 2007. Arch Intern Med 169:2071–2077
4. McCollough CH, Bruesewitz MR, Kofler JM (2006) CT dose reduction and dose management tools: overview of available options. Radiographics 26:503–512
5. Willemink MJ, de Jong PA, Leiner T, et al. (2013) Iterative reconstruction techniques for computed tomography part 1: technical principles. Eur Radiol 23:1623–1631
6. Willemink MJ, Leiner T, de Jong PA, et al. (2013) Iterative reconstruction techniques for computed tomography part 2: initial results in dose reduction and image quality. Eur Radiol 23:1632–1642
7. Yu MH, Lee JM, Yoon J-H, et al. (2013) Low tube voltage intermediate tube current liver MDCT: sinogram-affirmed iterative reconstruction algorithm for detection of hypervascular hepatocellular carcinoma. Am J Roentgenol 201:23–32
8. Chang W, Lee JM, Lee K, et al. (2013) Assessment of a model-based, iterative reconstruction algorithm (MBIR) regarding image quality and dose reduction in liver computed tomography. Invest Radiol 48:598–606
9. Schindera ST, Odedra D, Raza SA, et al. (2013) Iterative reconstruction algorithm for CT: can radiation dose be decreased while low-contrast detectability is preserved? Radiology 269:511–518
10. Vardhanabhuti V, Riordan RD, Mitchell GR, Hyde C, Roobottom CA (2014) Image comparative assessment using iterative reconstructions: clinical comparison of low-dose abdominal/pelvic computed tomography between adaptive statistical, model-based iterative reconstructions and traditional filtered back projection in 65 patients. Invest Radiol 49:209–216
11. Goenka AH, Herts BR, Obuchowski NA, et al. (2014) Effect of reduced radiation exposure and iterative reconstruction on detection of low-contrast low-attenuation lesions in an anthropomorphic liver phantom: an 18-reader study. Radiology 272:154–163
12. Park M, Chung YE, Lee HS, et al. (2014) Intraindividual comparison of diagnostic performance in patients with hepatic metastasis of full-dose standard and half-dose iterative reconstructions with dual-source abdominal computed tomography. Invest Radiol 49:195–200
13. Matsuki M, Murakami T, Juri H, Yoshikawa S, Narumi Y (2013) Impact of adaptive iterative dose reduction (AIDR) 3D on low-dose abdominal CT: comparison with routine-dose CT using filtered back projection. Acta Radiol 54:869–875
14. Geleijns J, Irwan R (2012) *Practical approaches to dose reduction: Toshiba perspective radiation dose from multidetector CT*. Berlin: Springer, pp 633–645
15. Yoon JH, Lee JM, Yu MH, et al. (2014) Comparison of iterative model-based reconstruction versus conventional filtered back projection and hybrid iterative reconstruction techniques: lesion conspicuity and influence of body size in anthropomorphic liver phantoms. J Comput Assist Tomogr. doi:10.1097/RCT.0000000000000145
16. Söderberg M, Gunnarsson M (2010) Automatic exposure control in computed tomography-an evaluation of systems from different manufacturers. Acta Radiol 51:625–634
17. Kim M, Lee JM, Yoon JH, et al. (2014) Adaptive iterative dose reduction algorithm in CT: effect on image quality compared with filtered back projection in body phantoms of different sizes. Korean J Radiol 15:195–204
18. Fletcher JG, Krueger WR, Hough DM, et al. (2013) Pilot study of detection, radiologist confidence and image quality with sinogram-affirmed iterative reconstruction at half-routine dose level. J Comput Assist Tomogr 37:203–211
19. Vardhanabhuti V, Loader R, Roobottom CA (2013) Assessment of image quality on effects of varying tube voltage and automatic tube current modulation with hybrid and pure iterative reconstruction techniques in abdominal/pelvic CT: a phantom study. Invest Radiol 48:167–174
20. Shuman WP, Green DE, Busey JM, et al. (2013) Model-based iterative reconstruction versus adaptive statistical iterative reconstruction and filtered back projection in liver 64-MDCT: focal lesion detection, lesion conspicuity, and image noise. Am J Roentgenol 200:1071–1076
21. Menke J (2005) Comparison of different body size parameters for individual dose adaptation in body CT of adults. Radiology 236:565–571
22. Gervaise A, Osemont B, Lecocq S, et al. (2012) CT image quality improvement using adaptive iterative dose reduction with wide-volume acquisition on 320-detector CT. Eur Radiol 22:295–301